

# Time-Dependent Dynamics in Networked Sensing and Control

Justin R. Hartman, Michael S. Branicky, and Vincenzo Liberatore

Electrical Engineering and Computer Science Department

Case Western Reserve University, Cleveland, OH 44106

`jjhartman@ra.rockwell.com`, `{mb,vincenzo.liberatore}@case.edu`

**Abstract**—A networked sensing and control system (NSCS) combines networked sensors with control and actuation units so as to control a physical environment. An NSCS can effectively use sensing and control signals only if those signals are delivered on time. The paper analyzes the behavior of an NSCS as a function of network real-time service. In particular, we consider the range of effective sampling periods and network delays that lead to stability for the controlled physical plant. A high-level conclusion is that the actual stability region is affected by the time-dependent behavior of packet delays and losses and can differ from an idealized stability region derived from an aggregate view of the loss and delay processes.

## I. INTRODUCTION

A *networked sensing and control system (NSCS)* combines networked sensors with control and actuation units so as to control a physical environment (Fig. 1). Applications are far-reaching and include, for example, industrial automation and distributed instrumentation [1]. A fundamental problem in NSCS is that sensor and control signals are useless or dangerous if they are delivered too late. In particular, a late control can jeopardize the stability, safety, and performance of the controlled physical environment. As a result, the physics of an NSCS critically depends on the real-time network behavior.

A broad research objective is to establish a methodology and the theoretical underpinnings of networked control [8]. In this paper, we analyze and simulate a representative physical system on simple topology. Our primary objective is to ascertain to what extent the complexity of time-varying network dynamics can be incorporated into a control-theoretical model. The paper focuses on packet-switched sensor networks because they are in widespread use in industrial automation and because the analysis is simpler than in an ad-hoc network.

In Section II, we introduce the NSCS that will be analyzed throughout the paper. Section III frames the main analytical properties of this NSCS, including the stability region and the traffic locus. In Section IV, we describe our co-simulation methodology. Section V gives the results of our co-simulations. Section VI concludes the paper.

For a fuller listing of works in the NSCS realm, consult the bibliography and the references contained herein, the thesis [5] from which this paper is condensed, or consult the papers and resources provided online in [8].

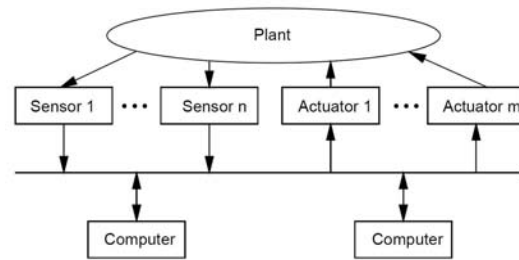


Fig. 1. Networked sensing and control system. Reproduced from [13].

## II. REPRESENTATIVE NETWORKED SENSING AND CONTROL SYSTEM

In this section, we introduce the networked sensing and control systems that will be used as examples throughout the paper. We will describe the architecture and parameters of the network through which the NSCSs will communicate. Additionally, we will describe an example nonlinear system.

### A. Network

The controller, sensors, and actuators of a networked sensing and control system are nodes on a computer network. Although there are many different physical and data link standards for networked control, we choose to focus on a simple and heterogeneous packet switched network, with no explicit quality-of-service (QoS) provisioning. Fig. 2 illustrates the topology of our sample network with three plants and a controller. The controller is at node 0, the router at node 1, and the plants at nodes 2, 3, and 4. Throughout the simulations, we vary many attributes of the network system, including: (i) the number of plants on the network, (ii) the size of the router's buffer at the T1 link, (iii) the delay of the T1 link.

Throughout this paper, we assume that the time required for the controller to calculate a control signal and initiate its transmission on the network is small enough to be ignored. In reality, however, some amount of time is required; this must be taken into consideration when choosing network parameters such as the number of plants which can be controlled by one controller.

In general, an NSCS will experience two distinct delays: a delay from the sensor to the controller ( $\tau_{sc}$ ), and a

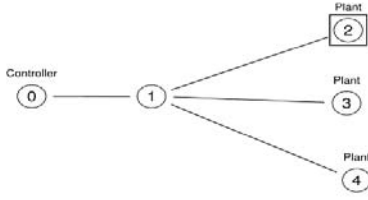


Fig. 2. Network topology with three plants.

delay from the controller to the actuator ( $\tau_{ca}$ ). Each can be analyzed using Eqs. (10) and (11) to find the bounds in which the the sensor-to-controller or controller-to-actuator delay will remain. Figure 3 illustrates the timing of the packets on an NSCS, including the sensor-to-controller and controller-to-actuator delays.

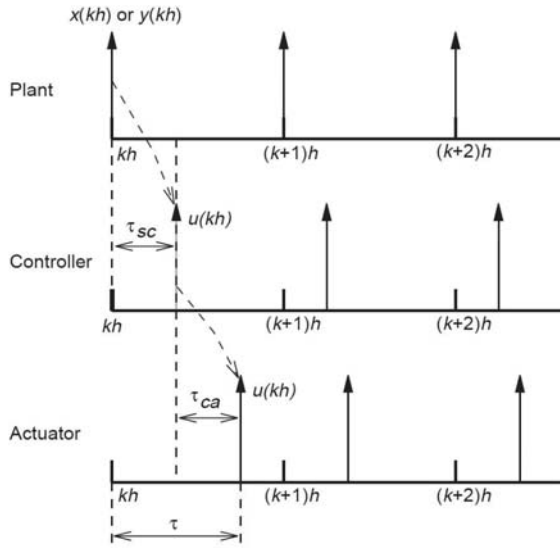


Fig. 3. Delay timing diagram for an NSCS. Reproduced from [14].

### B. Control System

We introduce and describe the system which will be used as an example: an inverted pendulum. It consists of a single point mass on the end of a rod, swinging freely from a cart on a track. Fig. 4 presents a cartoon of this system. The equations of motion for the inverted pendulum are:

$$\ddot{\phi} + \frac{3B_R}{4ML^2}\dot{\phi} - \frac{3g}{4L}\sin\phi = -\frac{3}{4L}\ddot{x}, \quad (1)$$

where  $B_R$  is the coefficient of friction of the pivot joint,  $M$  is the mass of the weight at the end of the rod,  $L$  is the length of the rod, and  $g$  is the gravitational constant. The input (control signal,  $u$ ) to the cart-mass system is the acceleration  $\ddot{x} = u$  of the cart, and the outputs are the angle of the pendulum,  $\phi$  (as measured from the “up” vertical position, with clockwise rotation being positive), and the position of the cart on the track,  $x$  (as measured from an arbitrary zero

location, with motion to the right being positive). For more details about the inverted pendulum, including Matlab code, see [3], [9], [11].

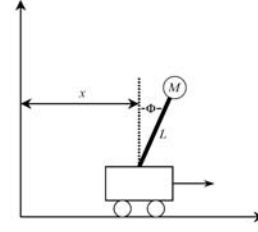


Fig. 4. Cartoon of inverted pendulum system. Modified from [11].

Once the system has been linearized, we can express it in state-space form, as in Eq. (2).

$$\begin{bmatrix} \frac{\delta x}{\delta t} \\ \frac{\delta \dot{x}}{\delta t} \\ \frac{\delta \phi}{\delta t} \\ \frac{\delta \dot{\phi}}{\delta t} \end{bmatrix} = \begin{bmatrix} 0 & 1 & 0 & 0 \\ 0 & 0 & 0 & 0 \\ 0 & 0 & 0 & 1 \\ 0 & 0 & \frac{3g}{4L} & -\frac{3B_R}{4ML^2} \end{bmatrix} \begin{bmatrix} x \\ \dot{x} \\ \phi \\ \dot{\phi} \end{bmatrix} + \begin{bmatrix} 0 \\ 1 \\ 0 \\ -\frac{3}{4L} \end{bmatrix} u. \quad (2)$$

When we sample a continuous-time system with a constant sampling period  $h$ , the resulting discrete-time system can be described by

$$x[k+1] = \Phi x[k] + \Gamma u[k], \quad (3)$$

where

$$\Phi = e^{Ah}, \quad \Gamma = \int_0^h e^{As} ds B. \quad (4)$$

Assuming the full state is available through sensors, a linear controller of the form  $u[k] = -Kx[k]$  can be designed to meet stability or performance objectives of the the overall, closed-loop system:

$$x[k+1] = \Phi x[k] - \Gamma K x[k] = (\Phi - \Gamma K)x[k]. \quad (5)$$

There are well-known methods (pole placement, LQR, etc.) that may be used to design  $K$  [4]. In this paper, we will primarily be concerned with the case where  $K$  is chosen such that the closed-loop system matrix  $\Phi - \Gamma K$  is *Schur* (i.e., all its eigenvalues have magnitude less than one).

## III. ANALYSIS

### A. Constant Network Delays

For networked sensing and control systems with fixed delays, we can analyze the system by reformulating the system matrices. Since the actuation of the system occurs at some time  $\tau$  after the controller has calculated the control signal, we must revise the system model to account for this delay. For delays less than one sampling period, and assuming a constant sampling period  $h$ , we can model the system as follows [4]:

$$x[k+1] = \Phi x[k] + \Gamma_0(\tau) u[k] + \Gamma_1(\tau) u[k-1], \quad (6)$$

where

$$\Phi = e^{Ah}, \quad \Gamma_0(\tau) = \int_0^{h-\tau} e^{As} B ds, \quad \Gamma_1(\tau) = \int_{h-\tau}^h e^{As} B ds. \quad (7)$$

By augmenting the system state space with the previous control signal value, we obtain  $\tilde{x}[k+1] = \tilde{A}\tilde{x}[k] + \tilde{B}u[k]$ , where

$$\tilde{A} = \begin{bmatrix} \Phi & \Gamma_1 \\ 0 & 0 \end{bmatrix}, \quad \tilde{B} = \begin{bmatrix} \Gamma_0 \\ 1 \end{bmatrix}, \quad \tilde{x}[k] = \begin{bmatrix} x[k] \\ u[k-1] \end{bmatrix}. \quad (8)$$

The stability of the system in Eq. (5) in an NSCS setting, sampled periodically with period  $h$  and subject to fixed delay  $\tau$ , can be assessed by testing the Schur-ness of the matrix

$$\tilde{A} - \tilde{B}[K \ 0]. \quad (9)$$

For delays greater than one sampling period, a similar process of augmenting the state space with more delayed control signals (e.g.  $u[k-2], \dots, u[k-n]$ ) can be used. For a fuller treatment of these techniques, see [13], [4].

In special cases (e.g., scheduled, no-collision transmissions on a private network), these methods are applicable. However, in NSCS involving the Internet, delays are in general unpredictable [6].

### B. Network Bottlenecks

Two of the primary difficulties in the analysis and design of networked sensing and control systems are packet loss and transmission delays. Some amount of delay is inherent in the data transmission across a network, and does not change; the portion of network-induced delay which can vary, as well as the phenomena of packet losses, are a result of collisions and queuing at intermediate nodes on a network. We investigate the primary causes of data loss and delay here.

In network devices (routers, switches, and hubs), the size of the link storage buffer is configurable. Hence, the maximum delay possible of an NSCS packet (traveling over a set of  $\mathcal{L}$  links from source to destination) is directly related to the size of the link buffers:

$$\tau_{\max} = \sum_{L \in \mathcal{L}} \left( \delta_L + \frac{8P(\beta_L + 1)}{\eta_L} \right), \quad (10)$$

where  $\delta_L$  is the fixed link delay of link  $L$ ,  $P$  is the packet size in bytes,  $\beta_L$  is the buffer size of link  $L$  in number of packets, and  $\eta_L$  is the link speed of link  $L$  in bits per second. (We assume for simplicity that all packets have the same size  $P$ . If the buffer size is expressed in bytes rather than the number of packets, one can simply use the packet size  $P$  to determine  $\beta_L$ .) Eq. (10) predicts that the maximum link delay increases with the buffer size. Of course, a smaller buffer also implies a larger number of packet losses.

The minimum delay for a network path is

$$\tau_{\min} = \sum_{L \in \mathcal{L}} \left( \delta_L + \frac{8P}{\eta_L} \right). \quad (11)$$

The delay for all packets in transit on the links in  $\mathcal{L}$  will be bounded by  $[\tau_{\min}, \tau_{\max}]$ .

### C. Varying Delay and Effective Sampling Period

The *effective sampling period* of an NSCS is the average sampling period of the NSCS over a period of time, taking into account all of the packet losses:

$$h_{\text{eff}}(t) = \frac{th}{t - hd(t)}, \quad (12)$$

where  $h$  is the nominal sampling period in seconds, and  $d(t)$  is the total number of packets belonging to the plant under observation dropped before time  $t$ .

If all the packets dropped on a link are due to over-saturation of the network, then we can use *a priori* knowledge of the network topology, link speeds, sampling periods, and data packet sizes to calculate the rate,  $r$ , at which control packets will be transmitted:

$$r = \min \left\{ \frac{\eta_L}{8E_T}, 1 \right\}, \quad (13)$$

where  $\eta_L$  is the link speed of the bottleneck link (in bits per second), and  $E_T$  is the number of bytes expected to arrive at the bottleneck link during one second of operation. For periodic traffic sources, we can replace  $E_T$  in Eq. (13) with a sum:  $E_T = \sum_{i \in \mathcal{N}} \frac{S_i}{h_i}$ , where  $S_i$  is the size of the periodic packet from the  $i^{\text{th}}$  node (in bytes),  $h_i$  is the transmission period of the  $i^{\text{th}}$  node, and  $\mathcal{N}$  is the set of all periodic nodes on the network.

Thus, given an expected usage pattern of the network, including all NSCSs and other regular periodic traffic sources, one can calculate an expected value of the transmission rate. Further, if we are given the transmission rate  $r$ , we can also calculate the effective sampling period,  $h_{\text{eff}}$ :

$$h_{\text{eff}} = \frac{h}{r} = \max \left\{ \frac{8h \sum_{i \in \mathcal{N}} \frac{S_i}{h_i}}{\eta_L}, h \right\}, \quad (14)$$

where  $h$  is the sampling period for which the plant was designed.

### D. Sampling Period and Delay Stability Region

For an ideal networked sensing and control system with no data loss and fixed delays, we can derive bounds on the sampling period and delay under which the system remains stable. By varying the sampling period and the constant delay of the system and testing the stability of the resulting system matrix (see Eq. (9)), we can plot the boundary of a region of stability, which we call the *sampling period and delay stability region (SPDSR)*. This idea was developed by Zhang *et al.* in [14], [13]; a generalized algorithm for discovering the SPDSR given continuous-time system matrices and a discrete-time feedback matrix is given in [5].

### E. Traffic Locus

A *traffic locus* is a locus of points describing, in the same sampling period and delay space as the stability regions, the theoretically possible points of effective sampling period and network-induced delay for a single plant, as a function of the amount of traffic on the network.

At all times, the packet delays on a network will be bounded by  $[\tau_{\min}, \tau_{\max}]$  from Eqs. (10) and (11). As long as the amount of traffic remains below the bandwidth of the network, the effective sampling period of a plant will be its actual sampling period, and the delay will remain fixed at  $\tau_{\min}$ . However, once the amount of traffic exceeds the network bandwidth, the delay will remain fixed at  $\tau_{\max}$  and the effective sampling period will increase. For networks where all nodes are periodic traffic sources, we can express the traffic locus as

$$T(h_{\text{eff}}) = \begin{cases} \frac{\tau_{\min}}{h_{\text{eff}}}, & \text{for } h_{\text{eff}} = h, \\ \frac{\tau_{\max}}{h_{\text{eff}}}, & \text{for } h_{\text{eff}} > h, \end{cases} \quad (15)$$

where  $h$  is the sampling period for which the plant was designed, and  $h_{\text{eff}}$  can be calculated from Eq. (14) for different amounts of network traffic.

## IV. CO-SIMULATION METHODOLOGY

### A. Network

In order to simulate a networked sensing and control system, the simulation of the dynamics of the state-space equations of a control system was combined with the simulation of a network topology into a single `ns-2` simulation script. This script utilizes the network components of `ns-2` to simulate network dynamics, such as the transmission, queuing, forwarding, and receipt of packets, as well as any network cross-traffic, such as FTP flows; the script also utilizes the Agent/Plant extension [2], [7] to simulate the sampling, control, and actuation of the control system components. The dynamics of each plant were simulated inline by first-order Euler approximations [5].

For these simulations, the controller is connected directly to a router by means of a T1 line, which has a bandwidth of 1.5 Mbps and a fixed link delay of 1 ms. Every other node on the network is a plant, which contains both the sensors for full-state feedback and the actuator for the control signal. All plant nodes are connected to the router via 10 Mbps links, with fixed link delays of 0.1 ms.

To illustrate the possible asymmetry of network delays, consider the sample network topology, where each link has a link buffer size of 50 packets. Using Eqs. (10) and (11), we discover that the sensor-to-controller and controller-to-actuator delays are bounded by

$$\begin{aligned} 1.494\text{ms} &\leq \tau_{\text{sc}} \leq 17.770\text{ms}, \\ 1.494\text{ms} &\leq \tau_{\text{ca}} \leq 3.936\text{ms}. \end{aligned}$$

In addition, if faster nodes flood the downstream T1 link to the controller, then the sensor-to-controller delay will be fixed at  $\tau_{\text{sc}, \max}$ . The controller, however, cannot flood the

faster outbound links; therefore, the controller-to-actuator delay will be fixed at  $\tau_{\text{ca}, \min}$ .

In addition to varying the network attributes listed above, we may wish to randomize or fix the scheduling of the plants' samples on the network. When we do not randomize the system sampling times, each plant uses the same sampling period for which it was designed, and the plants' samples are scheduled to be equidistant in time from one another within the sample period. More precisely, we choose the sampling period and sampling times of each plant be

$$h_i = H, \quad t_i[k] = \left(k + \frac{i-1}{N}\right) h_i, \quad (16)$$

where  $i \in \{1, \dots, N\}$ . Here,  $h_i$  is the sampling period of the  $i^{\text{th}}$  plant,  $t_i[k]$  is the absolute time of the  $k^{\text{th}}$  sample of the  $i^{\text{th}}$  plant,  $H$  is the sampling period for which the system was designed, and  $N$  is the total number of plants. When the sampling of the plants is fixed according to Eq. (16), it establishes a periodicity among the samples of all plants. It also provides the same amount of bandwidth to each plant on the network.

For no "overlap" of transmission times, one must assume, in addition to Eq. (16), that the transmission time of each packet is less than the bandwidth devoted to each packet. More precisely,

$$\frac{P}{\eta} < \frac{H}{N}, \quad (17)$$

where  $P$  is the size of the periodic NSCS packet,  $\eta$  is the bandwidth of the network path, and  $H$  and  $N$  are as before. If this assumption is not true, then we say the resulting network is *over-commissioned*; that is, the nodes commissioned on the network require more bandwidth than the network is able to provide. Such a situation will result in packet losses.

When the sampling times are randomized, each plant (with the exception of the first plant, which we are observing) chooses a sampling period up to 20% greater or less than the designed sampling period. In addition, the scheduling of the plants is randomized throughout the sampling period. Assuming there is no jitter in the plants' timing, we choose the sampling period and sampling times of the first plant in the same way as the non-randomized case of Eq. (16). Then for each plant  $i > 1$ , we choose two random variables,  $\rho_i \in [0.8, 1.2]$  and  $\psi_i \in [0, 1)$ , which represent the skew of the sampling period and the skew of the initial sample time, respectively, from a uniform distribution on their intervals. We then fix each plant's sampling period and sampling times as follows:

$$h_i = \rho_i H, \quad t_i[k] = (k + \psi_i) h_i. \quad (18)$$

When the sampling of the plants is randomized, it eliminates the periodicity found in the non-randomized sample schedules of Eq. (16); this better mirrors the real-world case where clock asynchronicity and skew cause aperiodic traffic sequences. Additionally, individual plants on the network

may be effectively allocated more or less bandwidth than the non-randomized case.

### B. Control System

The system contains nonlinearities, and we will linearize it for ease of analysis. However, we will simulate both linear and nonlinear system equations in order to observe the effects of the nonlinearity in the simulation results.

We have chosen values for the inverted pendulum system parameters:  $g = 9.8066 \text{ m/s}^2$ ,  $M = 8 \text{ kg}$ ,  $L = 0.125 \text{ m}$ ,  $B_R = 0.1$ . These parameters correspond to reasonable values in a physical implementation. The open loop system is unstable (poles at 0, 0, and  $\pm 8$ ) and controllable. We designed a full-state feedback controller for the inverted pendulum system to sample at a constant rate of 50 ms, which is used in the remainder of this paper:

$$K = \begin{bmatrix} -0.6673 & -1.1453 & -19.4454 & -2.4364 \end{bmatrix}. \quad (19)$$

This yields system poles at  $0.6809 \pm 0.0086i$  and  $0.9647 \pm 0.0340i$  for the closed-loop system matrix  $\Phi - \Gamma K$ . See [5] for details. For all simulations that follow, we use the initial condition  $(x, \dot{x}, \phi, \dot{\phi}) = (0, 0, -0.2095, -0.0977)$ .

While the analytic stability region can be informative, we wish to discover the stability region of a plant using the effective sampling period from Eq. (14). In order to do this, we must cause the NSCS to drop packets by over-saturating the network's bandwidth. Since the effective sampling period is directly proportional to the number of plants on the network, and the maximum delay of the link path is directly related to the router queue size, we can vary the number of plants and the router queue size to test different points in the sample space.

### C. Implementation

Simulations using the ns-2 network simulator used version 2.26, running in Cygwin version 1.5.5. Matlab-based calculations were done in Matlab 6.5.0.180913a Release 13. In all simulation results, we only tracked the state and output of the first plant in Fig. 2 (boxed node 2). For all other plants, only the network events are simulated; their dynamics are symmetric and hence not simulated, in order to conserve processor time during simulation.

## V. CO-SIMULATIONS

### A. Baseline

As a first step to understanding the influence of the control network on an NSCS, we compare the performance of the "ideal" NSCS against that of the non-networked, discrete-time system. We have simulated the inverted pendulum system with only one plant on the network, sampling at 50 ms, with no additional cross-traffic. Fig. 5 illustrates the system state of the baseline NSCS vs. the non-networked inverted pendulum system.

The baseline NSCS experiences small and constant sensor-to-controller and controller-to-actuator delays (about

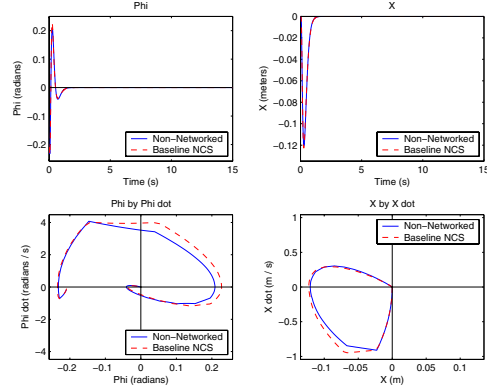


Fig. 5. Simulation of baseline inverted pendulum system.

1.5 ms each) due to the fixed propagation and transmission delays along the network paths. These delays cause the state of the inverted pendulum system to differ from that of the non-networked system at the same point in time. This difference in system state causes a difference in the control signal that is applied to the system.

### B. Many Plants

In the baseline NSCS simulations, the only nodes communicating on the network are the controller and the plant under observation. This configuration uses little of the system bandwidth, as the two nodes only exchange 64-byte packets every 50 ms (using 10 Kbps, which is approximately 0.65% of the available bandwidth). In order to use more of the network bandwidth, we will simulate the system with 147 NSCS plants communicating with the controller, which will utilize the total amount of bandwidth available on the T1 line. We fix the sample scheduling of the plants on the network according to the non-randomized scheme of Eq. (16). The performance of the inverted pendulum system with this configuration is very similar to that of the baseline system (data not shown).

When 147 plants communicate on the network, the bandwidth of the T1 line is slightly exceeded. Because of that, some sensor-to-controller packets are lost. Fig. 6 shows the control signal of this system, as well as the number of packets in the router queue, the number of packets lost at the T1 line buffer, and the sensor-to-controller and controller-to-actuator delays. As the queue begins to fill, the sensor-to-controller delay increases as incoming packets must wait for the queue to empty. Once the queue has filled, packets begin to be lost.

Although we are at the edge of bandwidth saturation, with time-varying delays and some packet loss, the pendulum shows performance similar to that of the baseline system.

### C. Over-Commissioned Network

In order to better simulate and analyze packet loss, we will study NSCSs which use more than the available bandwidth. If the network is over-commissioned in this

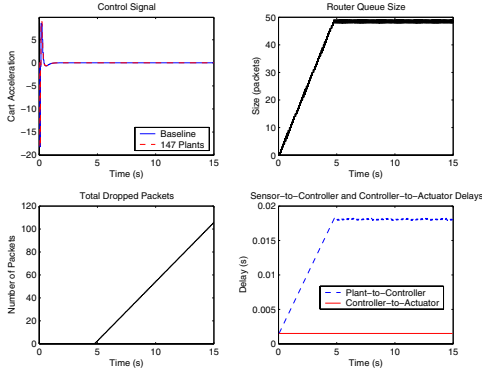


Fig. 6. Control signal, queue size, packet losses, and delays of the inverted pendulum system with 147 plants.

way, the network is guaranteed to lose packets; by varying the number of plants on the network, we can change the amount of sensor-to-controller packets which make it to the controller.

1) *Non-Randomized Sample Scheduling*: First, we fix the scheduling of the plants on the network according the non-randomized schedule of Eq. (16). This evenly distributes the amount of bandwidth per node. Fig. 7 illustrates the state of the inverted pendulum system with 175 plants with non-randomized sensor scheduling. Even though we are only slightly above the bandwidth of the T1 link, the system is already marginally stable, because the inverted pendulum system is sensitive to lost packets and long delays.

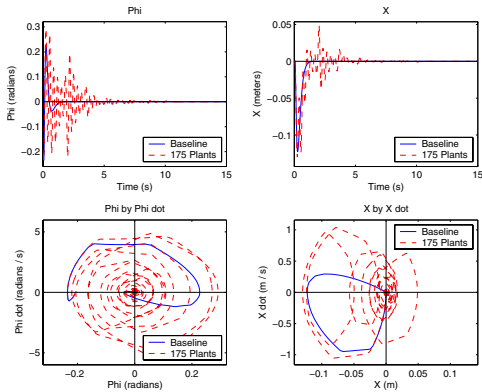


Fig. 7. Simulation of inverted pendulum on an over-commissioned network.

Fig. 8 shows the control signal and network dynamics of the inverted pendulum on an over-commissioned network. Because of the amount of traffic, the router queue fills quickly, and delays become high (18.23 ms) and nearly constant. Also, approximately 8.4% of the sensor-to-controller packets were lost.

2) *Randomized Sample Scheduling*: When the sampling of the sensors is randomly scheduled according to Eq. (18), the performance for the plant under observation can be

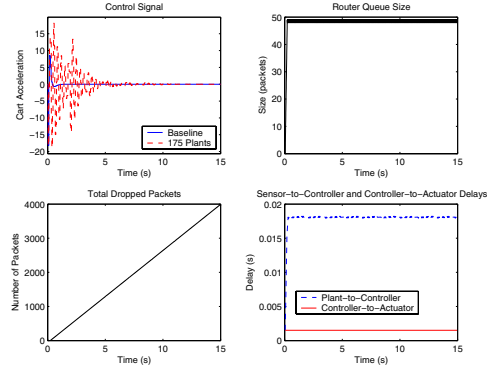


Fig. 8. Control signal, queue size, packet losses, and delays of the inverted pendulum system on an over-commissioned network.

better or worse than when it is not randomized, depending on the scheduled sampling times of the other plants. The performance and stability of an NSCS on an over-commissioned network with random scheduling is highly dependent on the sensitivity of the NSCS to packet loss and delay.

Fig. 9 illustrates the effective sampling of the first plant versus the number of plants on the network and the link buffer size. When the network is beyond saturation, the buffer is overflowed, and therefore changing the buffer size only increases the network-induced delay. However, as the number of plants increases, both packet losses and the effective sampling period increase.

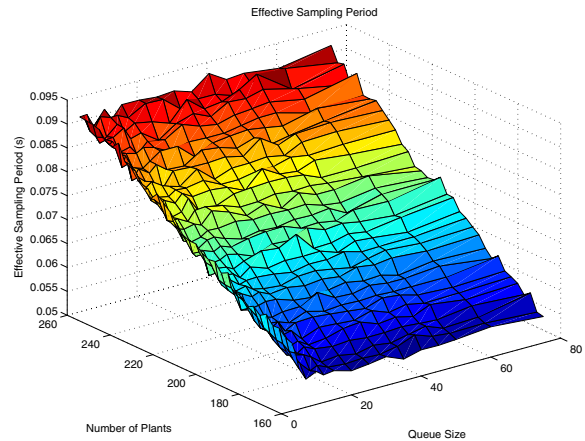


Fig. 9. Effective sampling period vs. number of plants, link buffer size.

The effective sampling period of Eq. (14) is the expected value over an infinitely long period, and with only periodic traffic sources. If other bursty traffic sources intermittently transmit on the network, then Eq. (14) under-estimates  $h_{\text{eff}}$ .

#### D. Stability Region

Fig. 10 (dotted line) is an analytical bound assuming a fixed-delay system with a fixed sampling period; Fig. 10 (solid line) simulates this by fixing the central link delay to

$\tau_{\min}$ , and changing the actual sampling period of the plant. Fig. 11 shows the analytical stability region from Fig. 10, along with the experimental stability region discovered by varying the buffer size and the number of plants on the network, which change both the maximum delay  $\tau_{\max}$  and the effective sampling period  $h_{\text{eff}}$ .

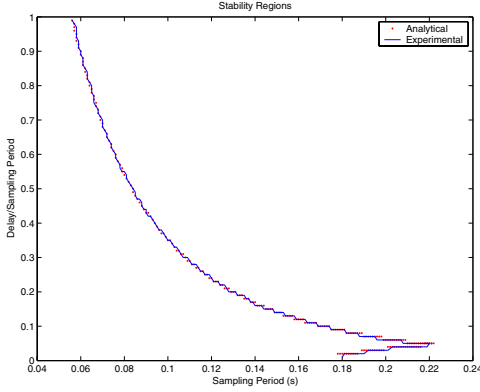


Fig. 10. Sampling period and delay stability region for the inverted pendulum: analytical and experimental from ns-2.

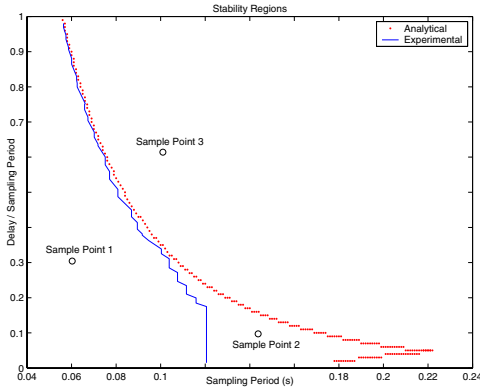


Fig. 11. Effective sampling period and maximum delay stability region for the inverted pendulum: analytical and from ns-2.

Because the analytical stability region is defined in terms of a constant sampling period and constant delay, it does not truly represent an NSCS. Under real network conditions, the delays of an NSCS will not be constant—they will vary randomly due to other traffic and collisions. Likewise, the sampling period will not vary linearly—rather, it will jump between discrete values ( $h[k] \in \{h, 2h, 3h, \dots\}$ ) for varying numbers of consecutively dropped packets. The theoretical stability region, then, is likely to be too liberal; this suspicion is confirmed in the region of Fig. 11.

We have chosen three points in the sampling period and delay space to illustrate the performance of the inverted pendulum system. At Sample Point 1, there are 176 inverted pendulum plants, and the T1 link has a buffer of 51 packets. The resulting effective sampling period is 60.282 ms, and the average delay is 18.342 ms. The performance of this

configuration is qualitatively the same as the baseline system (data not shown).

At Sample Point 2, there are 411 inverted pendulum plants on the network, and the T1 link buffer size is 38 packets. The resulting effective sampling period is 143.750 ms, and the average delay is 13.961 ms. Although this point is still within the SPDSR for the fixed delay and sampling period, the effective sampling period caused by packet loss causes it to become unstable (not shown).

At Sample Point 3, there are 294 plants on the network, and the T1 link buffer size is 180 packets. The resulting effective sampling period is 101.014 ms, and the average delay is 62.042 ms. This point is outside both stability regions, and the system is clearly unstable; see Fig. 12.

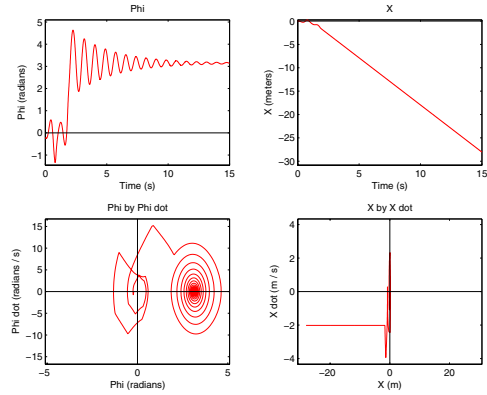


Fig. 12. Inverted pendulum system simulation at Sample Point 3.

### E. Traffic Locus

Since the delay in the sampling period and delay space is a fractional delay, this line actually traces a curve in the state space. Fig. 13 illustrates an example traffic locus for the inverted pendulum system. In this sample system, the queue size at the T1 boundary is fixed at 25; therefore, the maximum delay (using Eq. (10)) is 9.681 ms, and the minimum delay is 1.4744 ms. When the network bandwidth is below 100% utilization, the system can be represented by Sample Point 1, where  $h_{\text{eff}} = h = 0.05$  s, and  $T(h_{\text{eff}}) = T(h) = \frac{\tau_{\min}}{h_{\text{eff}}} = \frac{0.0014744}{0.05} = 0.0295$ . However, when traffic increases just beyond the saturation point of the T1 link (which occurs when there are 154 plants on the network),  $h_{\text{eff}} = 0.05013$ , the delay becomes  $\tau_{\max}$ , and  $T(0.0513) = \frac{0.009681}{0.0513} = 0.189$ , which is represented by Sample Point 2. As more plants are added the delay remains fixed at  $\tau_{\max}$ , more packets are dropped, and the effective sampling period increases. Sample Point 3 represents the system with 250 plants on the network, where  $h_{\text{eff}} = 0.08138$  and  $T(0.08138) = \frac{0.009681}{0.08138} = 0.119$ .

Fig. 14 illustrates a traffic locus for the inverted pendulum system with a router buffer size of 120, which makes  $\tau_{\max} = 40.606$  ms. Various numbers of NSCS plants are shown to illustrate the effect of increasing the amount of network traffic.



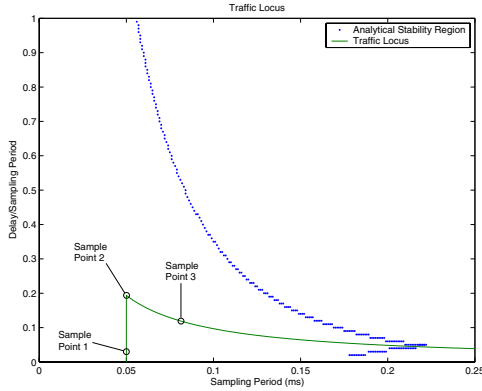


Fig. 13. Traffic locus for the inverted pendulum system (Queue size=25).

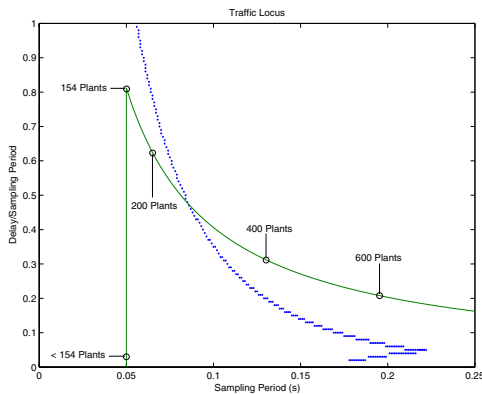


Fig. 14. Traffic locus for the inverted pendulum system (Queue size=120).

## VI. CONCLUSIONS

Sensor networks introduce non-trivial issues, such as routing, power management, and security. Networked Sensing and Control Systems are further complicated because the controlled physics depends on real-time communication properties.

Previous work highlighted the importance of the stability region to predict whether a NSCS is stable given the values of network delays and packet loss rates [14], [13]. The region often exhibits a non-convex shape (e.g., Fig. 10 and [14], [13]), which in turn can result in paradoxical behaviors. For example, a shorter delay can lead to an unstable system, while a longer one might re-stabilize it. The region can be computed numerically from average delay values and average loss rates. However, we also computed it directly through co-simulations, and the resulting region lacked the “non-convex tail” in this case (see Fig. 11). In other words, an accurate packet-level simulations removed the paradoxes implied by an average-case analysis. Our intuition is that the more surprising cases are in some sense associated with an “ill-defined” or “non-robust” system state, which disappears when network randomness is taken into account. A main conclusion of this paper is that the stability region must account for the exact network dynamics

to avoid the paradoxical effects that had been previously found in average-case analyses. In particular, these results give stronger support to a co-simulation methodology.

Additionally, we have explored the effect of adaptive and bursty data sources in [5]. The stability region for NSCSs was originally introduced in [14], [13].

Future work should address the use of analytical tools to calculate a bound similar to the experimental bound discovered in Fig. 11. Also relevant is the design of specific *compensation schemes* for NSCSs, that explicitly take into account delay and packet loss in crafting sensing and control policies. While preliminary work has been accomplished under various assumptions (see, e.g., [12], [10], [13], [5]), there are still many open problems.

## ACKNOWLEDGMENTS

This research was partially supported by the NSF (grant CCR-0309910); it does not necessarily reflect the views of the NSF. We would also like to acknowledge our colleague, Stephen Phillips, at ASU, who is a co-PI on the above grant. Mr. Hartman is currently with Rockwell Automation, 1 Allen Bradley Dr., Mayfield Heights, OH 44124.

## REFERENCES

- [1] A. Al-Hammouri, A. Covitch, D. Rosas, M. Kose, W. S. Newman, and V. Liberatore, Compliant Control and Software Agents for Internet Robotics, in *Eighth IEEE International Workshop on Object-oriented Real-time Dependable Systems (WORDS 2003)*, 280–287.
- [2] M. S. Branicky, V. Liberatore, and S. M. Phillips, “Networked Control System Co-Simulation for Co-Design,” in *Proc. American Control Conference*, Denver, USA, vol. 4, June 2003, pp. 3341–3346.
- [3] D. W. Deley, “Controlling an Inverted Pendulum: An Example of a Digital Feedback Control System,” WWW, Apr. 13, 2004, [members.cox.net/srice1/pendulum/synopsis.htm](http://members.cox.net/srice1/pendulum/synopsis.htm).
- [4] G. F. Franklin, J. D. Powell, and M. L. Workman, *Digital Control of Dynamic Systems*, 2nd ed. Reading, MA: Addison-Wesley, 1990.
- [5] J.R. Hartman, “Networked Control System Co-Simulation for Co-Design: Theory and Experiments,” M.S. thesis, Case Western Reserve University, Electrical Engineering and Computer Science, June 2004. [dora.case.edu/msb/pubs/jrhMS.pdf](http://dora.case.edu/msb/pubs/jrhMS.pdf).
- [6] J.F. Kurose and Keith W. Ross, *Computer Networking: A Top-Down Approach Featuring the Internet*, 2nd ed., Addison-Wesley, 2003.
- [7] V. Liberatore, “Network Control Systems,” WWW, December 2002, manual for Agent/Plant extension to ns-2, [home.case.edu/~vxl11/NetBots/ncs.pdf](http://home.case.edu/~vxl11/NetBots/ncs.pdf).
- [8] V. Liberatore, M. S. Branicky, S. M. Phillips, and P. Arora, “Networked Control Systems Repository,” WWW, May, 2004, [home.case.edu/ncs/](http://home.case.edu/ncs/).
- [9] B. Messner and D. Tilbury, “Control Tutorials for Matlab—Example: Modeling an Inverted Pendulum,” WWW, August 1997, [www.engin.umich.edu/group/ctm/examples/pend/invpen.html](http://www.engin.umich.edu/group/ctm/examples/pend/invpen.html).
- [10] J. Nilsson, “Real-Time Control Systems with Delays,” Ph.D. dissertation, Lund Institute of Technology, Automatic Control, Feb. 1998.
- [11] I. Tammeraid *et al.*, “Applications of Linear Algebra with Matlab—Example: A Cart and an Inverted Pendulum,” June 28, 1999, WWW, [www.cs.ut.ee/~toomas\\_l/linalg/matlabap/control/control12.html](http://www.cs.ut.ee/~toomas_l/linalg/matlabap/control/control12.html).
- [12] G. C. Walsh, H. Ye, and L. Bushnell, “Stability Analysis of Networked Control Systems,” in *Proc. American Control Conference*, San Diego, USA, June 1999, pp. 2876–2880.
- [13] W. Zhang, “Stability Analysis of Networked Control Systems,” Ph.D. dissertation, Case Western Reserve University, Electrical Engineering and Computer Science, May 2001.
- [14] W. Zhang, M. S. Branicky, and S. M. Phillips, “Stability of Networked Control Systems,” in *IEEE Control Systems Magazine*, vol. 21, no. 1, February 2001, pp. 84–99.